

Evidence of valence band perturbations in GaAsN/GaAs(001): Combined variable-angle spectroscopic ellipsometry and modulated photoreflectance investigation

S. Turcotte,¹ S. Larouche,¹ J.-N. Beaudry,¹ L. Martinu,¹ R. A. Masut,¹ P. Desjardins,¹ and R. Leonelli²

¹*Département de Génie Physique and Regroupement Québécois sur les Matériaux de Pointe (RQMP), École Polytechnique de Montréal, P.O. Box 6079, Station Centre-Ville, Montréal, Québec, Canada H3C 3A7*

²*Département de Physique and Regroupement Québécois sur les Matériaux de Pointe (RQMP), Université de Montréal, P.O. Box 6128, Station Centre-Ville, Montréal, Québec, Canada H3C 3J7*

(Received 24 June 2009; published 25 August 2009)

The contribution of the fundamental gap E_- as well as those of the $E_- + \Delta_{so}$ and E_+ transitions to the dielectric function of $\text{GaAs}_{1-x}\text{N}_x(001)$ alloys were determined from variable-angle spectroscopic ellipsometry and modulated photoreflectance spectroscopy analyses. The oscillator strength of the E_- optical transition increases weakly with nitrogen incorporation. The two experimental techniques independently reveal that the oscillator strength of the $E_- + \Delta_{so}$ transition becomes larger compared to that of the fundamental gap as the N content increases. Since the same conduction band is involved in both the E_- transition and its split-off replica $E_- + \Delta_{so}$, this result reveals that adding nitrogen in $\text{GaAs}_{1-x}\text{N}_x(001)$ alloys affects not only the conduction but also the valence bands.

DOI: 10.1103/PhysRevB.80.085203

PACS number(s): 78.20.Ci, 78.66.Fd

I. INTRODUCTION

The large band-gap reduction observed in III–V dilute nitride semiconductors is promising for various optoelectronic devices, such as photovoltaic cells,^{1,2} semiconductor lasers,^{3,4} photodiodes,⁵ and heterojunction bipolar transistors.^{6,7} In order to optimize the design of these devices, a better understanding of the optical properties, and, accordingly, of the optical constants (the dielectric function) and of the band structure of these materials is required.

In addition to significantly decreasing the band-gap energy, the incorporation of nitrogen in GaAs splits the conduction band into two nonparabolic subbands.^{8,9} A phenomenological model—the band anticrossing (BAC) model—has been successfully used to describe the direct gap transition energies associated with these subbands.¹⁰ The lower transition associated to the first conduction subband is labeled E_- , the next higher one E_+ , and the split-off transition $E_- + \Delta_{so}$. The BAC model is based on the observed apparent repulsion of those bands when the alloy is subjected to hydrostatic pressure.¹⁰ However, it oversimplifies the effects of N in III–V–N alloys by restricting the influence to the Γ symmetry point and by assuming that the valence bands remain unaffected.¹⁰ Surprisingly, the validity of this last assumption has not been systematically investigated even though some recent experimental results suggest a possible perturbation of the GaAsN valence bands.¹¹

Modulation techniques, such as electroreflectance,¹² photoreflectance¹³ (PR), and magnetotunneling spectroscopy,⁸ have been used for direct measurement of the optical transitions E_- and E_+ . Modulated reflectance methods, however, can only provide relative information on the band structure, such as the relative oscillator strength of the optical transitions. Francoeur *et al.*¹² reported that the E_+ transition involves the L critical point (CP) of the band structure. They proposed that breaking the translational symmetry by introducing nitrogen splits the degeneracy of the L conduction band and yields new transitions having an L_{6c} sym-

metry, including the optically active E_+ . Similar conclusions were also recently reached by Fluegel *et al.*¹⁴

The strength of the optical transitions in a semiconductor alloy can best be determined experimentally by extracting the dielectric function from spectroscopic ellipsometry measurements. Ellipsometric studies of the dielectric function of III–V–N semiconductor alloys have generally been done on a limited energy range^{15–18} while some, in addition, were based on a single angle of incidence.^{19–25} However, since the sample is a multilayered structure, it is recommended to expand the analysis to several angles of incidence. Using this approach, our group has recently shown that variable angle spectroscopic ellipsometry (VASE) has the required sensitivity to detect subtle transitions in GaAsN, such as the E_+ transition, allowing a comparison of the dielectric function with that obtained from first-principles calculations.²⁶ We used a point-by-point best match of the optical constants to confirm that the presence of the E_+ related transition, clearly identified in our VASE data, translates into significant contributions to the dielectric function.²⁶

In the present paper, we report a detailed study of the near-gap optical transitions E_- , $E_- + \Delta_{so}$, and E_+ from $\text{GaAs}_{1-x}\text{N}_x$ alloy epilayers grown on GaAs(001). Two complementary optical characterization techniques are used to analyze the effect of nitrogen incorporation on the optical properties of the alloys. The dielectric function is extracted from VASE measurements using a parametric model that is not subject to the noise associated with point-by-point best-match calculated data. The absorption coefficient at the direct band-gap edge, whose value is directly related to the oscillator strength of the lowest energy transition, is also deduced from the imaginary part of the dielectric function. Moreover, modulated photoreflectance measurements are used to independently determine the energy position and the relative oscillator strength of the E_- , $E_- + \Delta_{so}$, and E_+ transitions. These combined results reveal that the oscillator strength of the $E_- + \Delta_{so}$ transition becomes larger compared to that of the fundamental gap as the N content increases.

Since the same conduction band is involved in both the E_c transition and its split-off replica, the results demonstrate that adding nitrogen in $\text{GaAs}_{1-x}\text{N}_x$ alloys affects not only the conduction but also the valence bands.

II. EXPERIMENTAL DETAILS

$\text{GaAs}_{1-x}\text{N}_x$ samples were grown by organometallic vapor-phase epitaxy in a horizontal low-pressure cold-wall reactor equipped with a fast-switching run-vent manifold with minimized dead volume,²⁷ using Pd-purified hydrogen as the carrier gas, trimethylgallium as the group-III precursor, and tertiarybutylarsine and 1,1-dimethylhydrazine as group V sources. Growth temperatures of 550 and 575 °C were chosen since they allow controlled nitrogen incorporation over a relatively wide composition range while maintaining sharp optical features. Our samples consist of nominally undoped $\text{GaAs}_{1-x}\text{N}_x$ layers $0.004 \leq x \leq 0.016$ deposited on a 50–100-nm-thick GaAs buffer layer grown on semi-insulating GaAs(001) substrates. The nitrogen composition x was determined from high-resolution x-ray diffraction (HR-XRD) measurements, based on a recent investigation which revealed that Vegard's rule applies in $\text{GaAs}_{1-x}\text{N}_x/\text{GaAs}(001)$ samples for up to $x \approx 0.03$.²⁸ The HR-XRD measurements were carried out in a Philips diffractometer using $\text{Cu } K\alpha_1$ radiation ($\lambda = 0.154\,059\,7$ nm) from a four-crystal Ge(220) Bartels monochromator which provides an angular divergence of 12 arc s with a relative wavelength spread $\Delta\lambda/\lambda = 7 \times 10^{-5}$. ω - 2θ scans (where ω is the angle of incidence and θ is the Bragg angle) were obtained with a detector acceptance angle of approximately 2°. Further details concerning the growth procedure and structural characterization can be found in Ref. 28.

PR measurements have been performed at room temperature using a 0.26 m Oriel spectrometer. The monochromatized light of a halogen lamp passing through the spectrometer provided the probe beam. The probe power density at the sample was around 0.2 mW cm^{-2} . The wavelength step was set to 5 meV (the resulting bandwidth resolution ranges from 5 meV at 1.35 eV to 9 meV at 1.8 eV). A 25 mW laser emitting at a wavelength of 405 nm was used to modulate the reflectance. Its power density was set between 16 and 140 mW cm^{-2} using neutral density filters in order to minimize Franz-Keldysh effects while providing a sufficiently high signal from the transitions probed.

Ellipsometric measurements were carried out at room temperature using a J.A. Woollam Co. vertical VASE apparatus fitted with a rotating analyzer.^{29,30} Since ellipsometry measures the ratio of the parallel to perpendicular amplitude reflection coefficients, no signal modulation is used in this technique, comparatively to PR. A xenon short-arc lamp was used as the light source. A systematic calibration is done at 500 and 1177 nm using a thermally oxidized SiO_2/Si reference sample before each measurement run. This procedure ensures the correct determination of the angular position of the input polarizer and of the output analyzer with respect with the plane of incidence and is needed to obtain accurate values of the ellipsometric angles during the spectroscopic experiment. In all cases, a low noise level (typical normal-

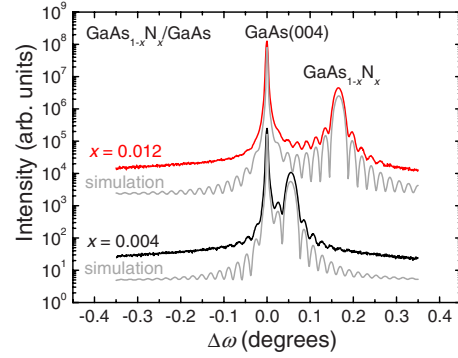


FIG. 1. (Color online) ω - 2θ HR-XRD scans through the 004 Bragg peak from $\text{GaAs}_{1-x}\text{N}_x/\text{GaAs}(001)$ samples with $x=0.004$ and 0.012. Fully dynamical simulations of the HR-XRD ω - 2θ scans are shown for comparison. Curves are shifted vertically for clarity.

ized chi squared less than 2) was obtained. A relatively large spot size (~ 1 mm in diameter or more) provided a large signal-to-noise ratio. The measurements cover the available light-source range which extends from 0.76 to 4.40 eV in order to include most optical transitions that are affected by the presence of nitrogen in $\text{GaAs}_{1-x}\text{N}_x$ alloys. The measurement energy step was set to 20 meV or better. For higher energies, the resolution is limited by the 6 nm light bandwidth of the ellipsometric apparatus (corresponding to 3 meV at 0.76 eV and 26 meV at 2.3 eV). Measurements were carried out at four or five angles of incidence near the GaAs Brewster angle ($\sim 74^\circ$); a 0.5° interval between the various angles of incidence was found to result in significant differences in ellipsometric variables ψ and Δ . The samples were cleaned using hot acetone, hot propanol, and deionized water and dried with nitrogen before optical measurements.

III. RESULTS

Figure 1 shows typical HR-XRD ω - 2θ scans obtained for the 004 Bragg peak from two samples used in this study (here for $x=0.004$ and 0.012). The scans exhibit sharp substrate and layer peaks. Furthermore, finite-thickness interference fringes are clearly visible in both scans, indicating that these alloy layers are of high structural quality with laterally uniform buffer-layer/film interfaces.

Simulated HR-XRD scans, based on the fully dynamical formalism of Takagi³¹ and Taupin³² are shown in Fig. 1 for comparison with experimental data. The simulations were carried out assuming perfectly abrupt and coherent interfaces, and linearly interpolated elastic constants.³³ The measured and simulated curves are in good agreement with respect to the angular position and relative intensities of both the diffraction peaks and the interference fringes. Nitrogen compositions extracted from the analysis of HR-XRD scans assuming Vegard's rule are reported in Table I for all samples. The $\text{GaAs}_x\text{N}_{1-x}$ layer thicknesses indicated in Table I were determined from HR-XRD (matching the spacing of the finite-thickness interference fringes in experimental and simulated curves) in the case of the thinner samples. For thicker films, thicknesses are obtained by modeling the re-

TABLE I. GaAs_{1-x}N_x layer parameters.

x	Thickness from HR-XRD (nm)	Starting value of the thickness from the best-match calculated data of the interference fringes (nm) ^a	Incident angles covered during VASE measurements (deg)
0 (GaAs)	N/A		73.6–75.6
0.004	253 ± 6		73.9–75.4
0.0066		2279 ± 5	73.8–75.3
0.012	243 ± 6		73.6–75.6
0.016		1206 ± 1	73.8–75.3

^aReference 44

fractive index dispersion that gives rise to the interference fringes visible in the transparent region of the ellipsometric data. The presence of the interference fringes in either HRXRD or VASE data, for thinner and thicker layers, respectively, indicates that the GaAsN films were uniform in thickness and in composition. The HRXRD analysis also confirms that the thinner films are fully strained and that strain relaxation remains below 25% in the thicker samples.

Figure 2 presents room-temperature PR spectra from the samples listed in Table I. The E_- (and thus the $E_- + \Delta_{so}$) and E_+ transitions can be identified since they shift, as expected, to lower and higher energies, respectively, with increasing N content. The absence of Franz-Keldysh oscillations together with the relative changes in reflectance $\Delta R/R$ of $\approx 10^{-4}$ are strong indications that low-field conditions are met in these spectra.³⁴ The PR line shapes of each transition can, therefore, be analyzed using the low-field formula^{35,36}

$$\frac{\Delta R}{R} = C \gamma^n \operatorname{Re}[e^{i\varphi}(E - E_t + i\gamma)^{-n}], \quad (1)$$

where C is a constant, γ is the line broadening, E_t is the transition energy, φ is the line-shape phase angle that accounts for the influence of nonuniformity in the electric fields, and n is a parameter that depends on the type of CP. For three-dimensional CPs, $n=2.5$.³⁷ The spectral features associated with the E_- , $E_- + \Delta_{so}$, and E_+ transitions were best matched using Eq. (1) and a least-squares minimization procedure. Experimental and best-match curves are in excellent agreement for all transitions in all samples as depicted in Fig. 3. The parameters obtained for the best-match calculated data are given in Table II.

The energies of the three main transitions extracted from the PR best-match calculated data are plotted as a function of N content in Fig. 4 and compared with the predictions of the BAC model. The variations in the fundamental band gap and of its split-off replica with N composition are in good agreement with the BAC model predictions. However, while this model predicts that the E_+ transition shifts to higher energies in a quadratic way, our results rather indicate a linear blue-shift with N incorporation as was also determined from measurements performed at 80 K (Ref. 12) and 10 K.¹⁴ The linear regression intercepts the ordinate axis at 1.75 ± 0.01 eV, which lies 1.16 eV below the room-temperature GaAs E_1 transition energy.^{38,39} This value is in

agreement with that found by Francoeur *et al.*¹² at a lower temperature and corroborates the L nature of the E_+ transition.

Experimental VASE data are presented as ψ and Δ spectra in Fig. 5 for a GaAs substrate and for GaAs_{1-x}N_x samples with $x=0.004$ –0.016. The E_- and $E_- + \Delta_{so}$ features are high-

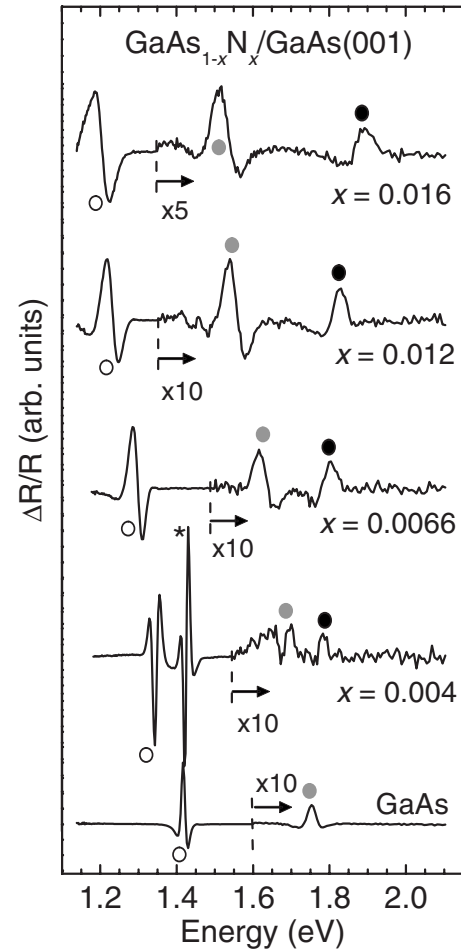


FIG. 2. Room-temperature PR spectra from a reference GaAs substrate and from GaAs_{1-x}N_x/GaAs(001) samples with $x=0.004$ –0.016. The E_- , $E_- + \Delta_{so}$, and E_+ transitions are identified with open, gray, and black circles, respectively. The feature identified by a star for the sample with $x=0.004$ is related to the band-gap edge of the underlying GaAs substrate.

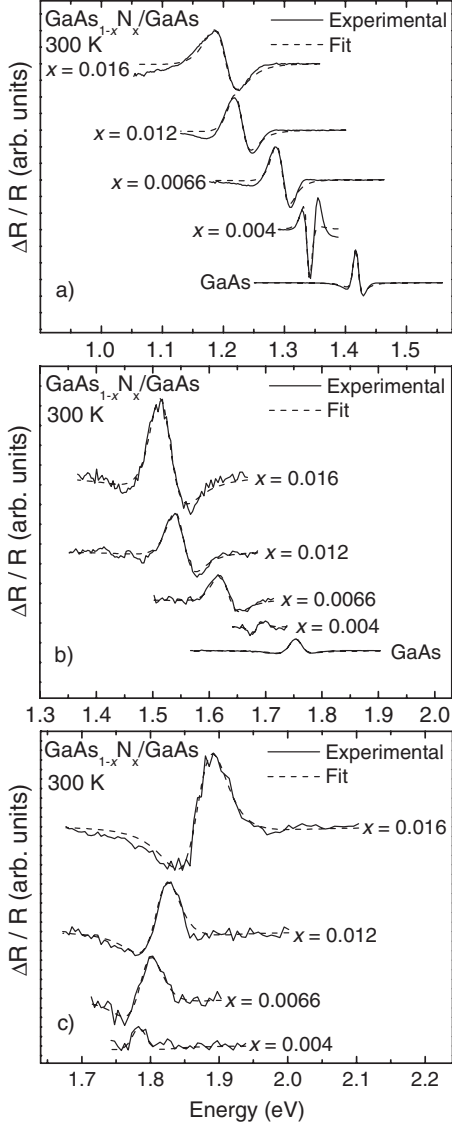


FIG. 3. Experimental PR spectra (solid lines) and best-match PR calculated data (dashed lines) from $\text{GaAs}_{1-x}\text{N}_x/\text{GaAs}(001)$ samples with $x=0.004\text{--}0.016$. The energy scales were selected to cover the (a) E_- , (b) $E_- + \Delta_{\text{so}}$, and (c) E_+ transitions.

TABLE II. Best-match calculation parameters (C , γ , and E_t) used for the low-field modeling of the main transitions (E_- , $E_- + \Delta_{\text{so}}$, and E_+) visible in PR spectra. The estimated uncertainties in the values for the amplitude and the broadening are $\pm 2\%$ and ± 0.8 meV, respectively, while they are well within ± 5 meV for the transition energies.

x	E_- (E_0 for GaAs)			$E_- + \Delta_{\text{so}}$ ($E_0 + \Delta_{\text{so}}$ for GaAs)			E_+		
	C	γ (meV)	E_t (eV)	C	γ (meV)	E_t (eV)	C	γ (meV)	E_t (eV)
0.0	1.09	10.2	1.418	0.0308	25.7	1.752			
0.004	1.66	9.5	1.339	0.0224	19.0	1.682	0.0189	27.1	1.784
0.0066	1.30	21.7	1.295	0.0684	35.4	1.627	0.0469	39.2	1.793
0.012	1.22	26.9	1.226	0.112	37.0	1.548	0.0563	42.5	1.817
0.016	1.30	39.6	1.200	0.206	45.3	1.519	0.0895	51.2	1.875

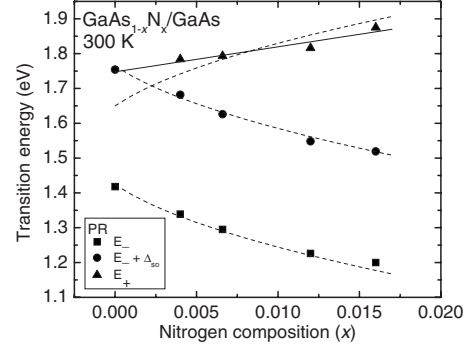


FIG. 4. Transition energies obtained from the best-match PR calculated data in Fig. 3 using Eq. (1). Dashed lines correspond to the predictions of the BAC model whereas the solid line is a linear regression of the E_+ experimental data.

lighted using gray and black vertical lines, respectively. One should already note that these features are visible for all angles of incidence. While the E_- CP is easily distinguished, the $E_- + \Delta_{\text{so}}$ CP is broader and more subtle. As the N content increases, the E_- and $E_- + \Delta_{\text{so}}$ transitions redshift and a feature, indicated with a vertical dashed line, gradually emerges in all ψ and Δ spectra. This feature shifts to higher energies with increasing N content while the E_- and $E_- + \Delta_{\text{so}}$ CP continue to redshift. For completeness, we have verified that a feature that blueshifts with nitrogen composition is present in the pseudodielectric function of the dilute nitrides samples studied.⁴⁰ No intermediate transition exists between $E_0 + \Delta_{\text{so}}$ and E_1 in nitrogen-free GaAs and one must therefore consider an additional CP in the analysis of the VASE data from $\text{GaAs}_{1-x}\text{N}_x$ samples. As its energy position closely matches that of E_+ observed in PR spectra, we attribute this feature to the E_+ transition.

IV. DISCUSSION

A. Determination of the dielectric function from VASE data

In order to extract the dielectric function from the VASE data, we developed a bilayer-substrate model reproducing the measured ψ and Δ spectra acquired at different angles of incidence. The GaAs substrate is assumed to be semi-infinite and comprises the GaAs buffer layer since the optical prop-

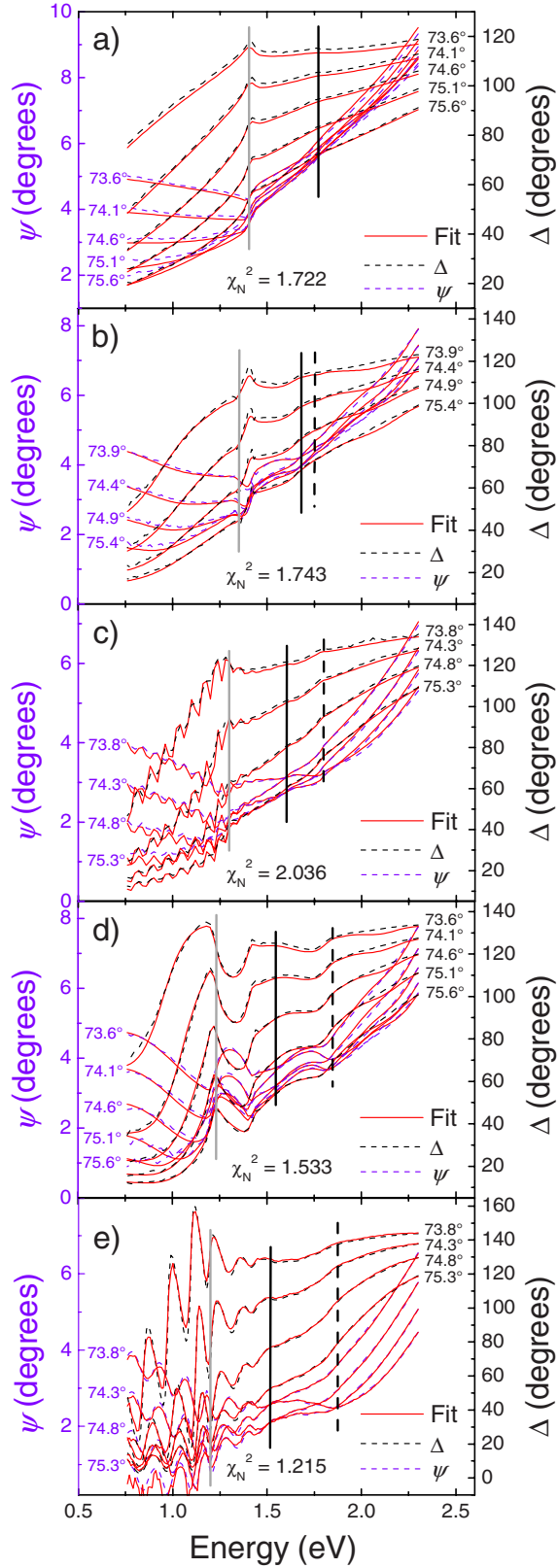


FIG. 5. (Color online) Experimental VASE spectra (dashed lines) and best-match VASE calculated data (solid lines) for $\text{GaAs}_{1-x}\text{N}_x$ samples with (a) $x=0$ (substrate), (b) $x=0.004$, (c) $x=0.0066$, (d) $x=0.012$, and (e) $x=0.016$. The vertical gray and black lines correspond to the E_- and $E_- + \Delta_{\text{so}}$ transitions, respectively. The black dashed line reveals the E_+ transition in the dilute nitride samples.

erties of both layers are essentially identical for the purpose of this analysis. We then consider the dilute nitride layer and an oxide overlayer which we assume to be a typical GaAs native oxide.

The parametric model of Herzinger and co-workers,⁴¹ which is inspired from that of Kim *et al.*,⁴² is used in the WVASE 32 software to model the complex dielectric function $\varepsilon = \varepsilon_1 + i\varepsilon_2$ from the VASE spectra. In this framework, each CP is parameterized by its center energy position, its magnitude, and its width, assuming a Gaussian broadening. For each sample, we begin by matching the spectra for energies below 2.3 eV for the corresponding GaAs substrate covered with a native oxide.⁴³ The values deduced for the GaAs substrate are then used for the substrate portion of the bilayer-substrate ellipsometric model of the nitride sample.

Then, an initial determination of the $\text{GaAs}_{1-x}\text{N}_x$ and oxide layer thicknesses is obtained. For thick samples, we modeled the dispersion of the index of refraction at energies below that of the $\text{GaAs}_{1-x}\text{N}_x$ band gap using the Cauchy dispersion model⁴⁴ in order to reproduce the interference fringes and obtain the thickness of the $\text{GaAs}_{1-x}\text{N}_x$ layers. For thin samples in which these interferences are too wide in energy to be matched in the raw ellipsometric data, we used the thickness obtained from Pendellösung fringes in the HR-XRD spectra as starting values.

The process of determining the dielectric function of the nitride layer begins with a rough best-match calculation of the whole spectra (0.76–4.40 eV) by changing only the E_1 and $E_1 + \Delta_1$ transition parameters of the $\text{GaAs}_{1-x}\text{N}_x$ layer (using the GaAs values as starting points). Since these transitions dominate and are clearly affected by N incorporation,⁴⁵ this ensures that the low-energy side of the E_1 transition is accurately described. Then, the energy, the amplitude, and the broadening of the three transitions (E_- , $E_- + \Delta_{\text{so}}$, and E_+) occurring below 2.3 eV are allowed to vary in a series of steps where the high-energy tail of each CP is also adjusted. We first determine the best-match values of the parameters for the E_- transition, which has the most effect on that portion of the spectra. The parameter values for the $E_- + \Delta_{\text{so}}$ and E_+ transitions are then adjusted. Focusing on the energy range 0.76–2.3 eV enables one to concentrate the matching procedure on the relevant transitions and to reduce the number of parameters.⁴⁶ For each sample, we adjust the modeled spectra to reproduce all acquisition angles by imposing the same set of parameters.

Differences between the measured and calculated ψ and Δ spectra are minimized using the Levenberg-Marquard algorithm. Qualitative information on the quality of the best-match calculated data is provided by the normalized chi-squared χ_N^2 , whose value stays below 2.0 for every sample. The results of the modeling procedure are presented in Fig. 5. Further, the fact that the modeled ψ and Δ curves reproduce well the shapes of the different ellipsometric features associated with the three main transitions E_- , $E_- + \Delta_{\text{so}}$, and E_+ for all samples demonstrates the suitability of the model. The resulting parameters leading to the best match between the modeled and experimental curves are given in Table III. For the sample with $x=0.004$, the E_+ and the $E_- + \Delta_{\text{so}}$ transitions are so close in energy that they appear indistinguishable from the raw ψ and Δ spectra. In this case, the two transi-

TABLE III. GaAs_{1-x}N_x VASE best-match calculation parameters: amplitude, broadening, and energy position are given for the three main transitions. The last column gives the relative oscillator strength S_{rel} for the $E_- + \Delta_{so}$ transition. The estimated uncertainties in the values for transition energies are ± 10 meV for the E_- transition and ± 20 meV for the $E_- + \Delta_{so}$ and the E_+ transitions. For the amplitudes, the uncertainties are ± 0.005 , ± 0.01 , and ± 0.004 for the E_- , $E_- + \Delta_{so}$, and E_+ transitions, respectively. The broadening uncertainty is ± 7 meV for the E_- transition. For the subtle $E_- + \Delta_{so}$ and the E_+ transitions, it is estimated to be on the order of the broadening value.

x	Amplitude (arbitrary units)			Broadening (meV)			Energy position (eV)			S_{rel}
	E_-	$E_- + \Delta_{so}$	E_+	E_-	$E_- + \Delta_{so}$	E_+	E_-	$E_- + \Delta_{so}$	E_+	
0	0.306	0.10		20	50		1.412	1.769 ^a		0.32
0.004	0.290	0.09	0.052	41	40	15	1.339	1.682	1.747	0.29
0.0066	0.340	0.15 ^b	0.069	56	33	13	1.295	1.615	1.793	0.44
0.012	0.314	0.18	0.077	20	78	27	1.226	1.548	1.856	0.56
0.016	0.330	0.30	0.008 ^c	20	77	23	1.200	1.519	1.875	0.91

^aThe uncertainty on this parameter is ± 30 meV.

^bThe uncertainty on this parameter is ± 0.05 .

^cThis E_+ feature merges with E_1 and $E_1 + \Delta_1$.

tions were resolved in the third derivative of ψ and Δ . We verified that two separate CPs are needed to reproduce those features.

The parameters of the ellipsometric model are used to determine the unique values of ε_1 and ε_2 which will provide the best match to the ψ and Δ spectra for the available angles of incidence. The relationship between ε_1 , ε_2 , ψ , Δ , and the angle of incidence is established using a multilayer model built from the Fresnel equations for the polarizations parallel and perpendicular to the incidence plane.⁴⁷ Real (ε_1) and imaginary (ε_2) parts of the dielectric function obtained from modeling the VASE data are presented in Fig. 6 for all GaAs_{1-x}N_x samples. In this figure, one can already observe that the contributions of E_+ and $E_- + \Delta_{so}$ to ε_2 increase with nitrogen content. Figure 6 and Table III also reveal that the contribution of the E_+ transition to ε_2 is almost lost for $x = 0.016$. We attribute this behavior to the broadening of the intense L -point E_1 and $E_1 + \Delta_1$ transitions that already dominate the GaAs (ε_2) (up to ~ 3.5 eV). For instance, focusing on the E_1 transition, we measure that the ε_2 maximum is 60 times larger than at the E_0 edge in GaAs. Upon nitrogen addition to the GaAs lattice, these transitions broaden considerably to become almost undistinguishable, as shown in the inset of Fig. 6(b), in agreement with other ellipsometry studies.^{18–20,23–25,48–50} Therefore, for the sample with $x = 0.016$, the E_+ blueshift is the largest and the E_+ transition becomes masked by the dominant contributions of the L -related transitions.

The nitrogen induced breaking of symmetry also leads to a splitting of the first conduction band of the L CP.^{12,51} However, the resulting additional transition that would appear near the E_1 transition might be difficult to observe due to the weaker effect of nitrogen on the E_1 transition than on the E_- and E_+ transitions.⁵²

The specific behavior of the oscillator strength of the E_- transition itself can be best represented by the absorption coefficient spectra near threshold, which we derived from the dielectric function of each GaAsN layer obtained by modeling and which is plotted in Fig. 7. First, the absorption coef-

ficients at threshold in GaAsN are comparable to that of GaAs (~ 7900 cm⁻¹ at threshold).⁵³ Second, we find that they slightly increase with nitrogen content over the entire composition range investigated, in qualitative agreement with previous reports.⁵⁴ We draw upon these observations in the conclusion section.

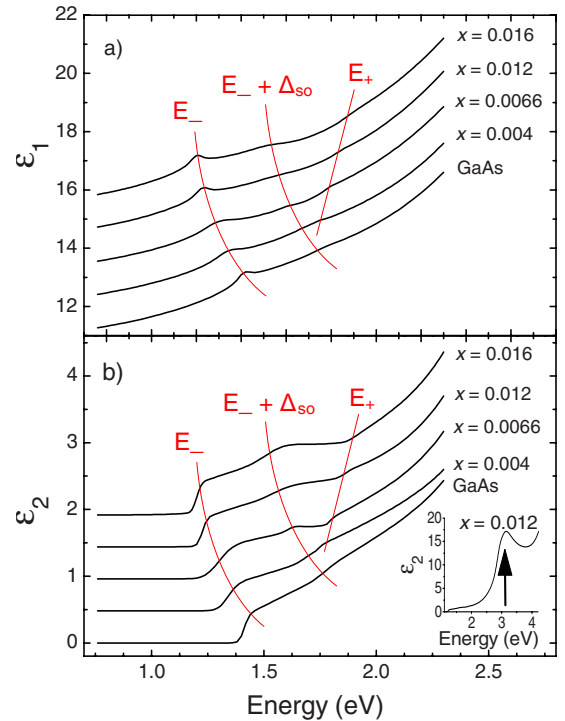


FIG. 6. (Color online) (a) Real and (b) imaginary parts of the dielectric function of GaAs_{1-x}N_x layers. The curves have been vertically shifted for clarity. Lines are guides to the eyes. The inset in (b) shows the imaginary part of the dielectric function for the sample with $x = 0.012$, in a wider energy range. The arrow highlights the peak around which the L -related E_1 and $E_1 + \Delta_1$ transitions are located.

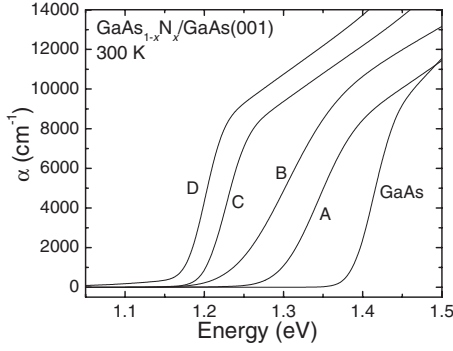


FIG. 7. Absorption coefficient at 300 K at the E_- threshold for $\text{GaAs}_{1-x}\text{N}_x$ samples deduced from the ellipsometric analysis for (A) $x=0.004$, (B) $x=0.0066$, (C) $x=0.012$, and (D) $x=0.016$. The spectrum from the GaAs substrate is also presented for reference.

B. Relative oscillator strength

Examination of Table II reveals that the E_+ transition is well distinguished from the split-off transition of the $\text{GaAs}_{1-x}\text{N}_x$ epilayer. As expected, the E_+ transition blueshifts while the E_- and $E_+\Delta_{so}$ transitions redshift with nitrogen incorporation. The energy difference between the $E_+\Delta_{so}$ and E_- transitions, however, slowly decreases with increasing nitrogen, as can also be observed from the data in Ref. 12, at 80 K. In order to further investigate the evolution of these three main transitions, we revisit the PR results, by taking the modulus of Eq. (1)

$$\left| \frac{\Delta R}{R} \right| = \frac{C\gamma^n}{[(E - E_t)^2 + \gamma^2]^{n/2}}. \quad (2)$$

Equation (2) describes an $n/2$ -order Lorentzian with an approximate width of 2γ . The integrated area is proportional to the PR oscillator strength of the transition.⁵⁵ Within a very good approximation, this area is proportional to $C\gamma$. As seen in Table II, it differs widely from sample to sample. To extract quantitative information from this data, it is better to introduce the relative PR oscillator strength O_{rel} of a given transition t with respect to the fundamental band-gap transition, which we define as

$$O_{rel} = \frac{C_t \gamma_t}{C_{E_-} \gamma_{E_-}}. \quad (3)$$

A quantitative evaluation of the oscillator strength of the various transitions can also be extracted from the VASE results. The parametric model described above being an extension of critical-point parabolic band models,⁴² the amplitude parameter of the related transition gives the oscillator strength of the transition.^{41,47} The relative oscillator strength S_{rel} for a given transition t observed in the ellipsometric measurements is then obtained from the ratio of its amplitude and that of the band edge.

Figure 8(a) presents both relative PR strength O_{rel} (scale to the left) and S_{rel} (right scale) as a function of the nitrogen fraction x for the E_+ transition. They both show a rapid rise for $x \sim 0.005$, followed by a lower rate of increase for higher N content. This near saturation is consistent with *ab initio* calculations of the ϵ_2 spectrum of $\text{GaAs}_{1-x}\text{N}_x$.²⁶ The PR

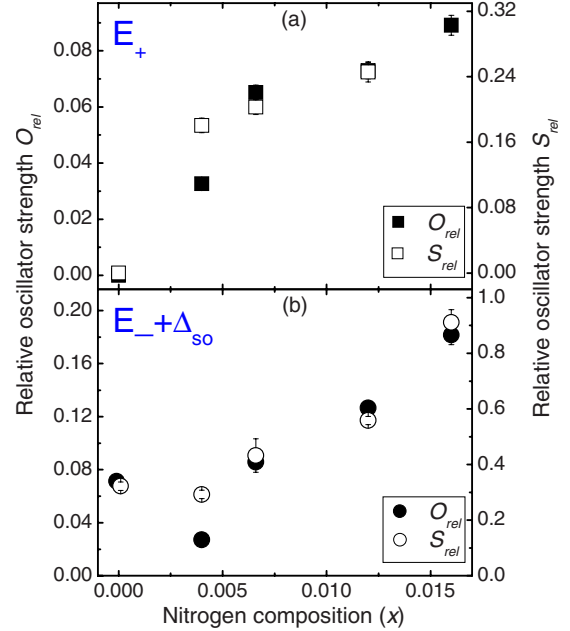


FIG. 8. (Color online) Relative oscillator strength O_{rel} (solid symbols) and S_{rel} (open symbols) versus nitrogen fraction x for (a) the E_+ transition and (b) the $E_+\Delta_{so}$ transition.

spectra being the result of many convoluted factors involving the reaction of the electronic structure to a modulated electric field, it is not surprising to observe that the actual values of O_{rel} and S_{rel} do not coincide. Nevertheless, the same trend and near saturation of the oscillator strength is observed for both results.

Figure 8(b) shows both oscillator strengths as a function of x for the $E_+\Delta_{so}$ transition. The trends shown by the two sets of data are again in very good agreement. Furthermore, the magnitude of the PR values agrees well with those reported in Ref. 11. The dielectric function of the GaAs reference sample shown in Fig. 6 is also in good agreement with reported data,^{19,38} the oscillator strength for the split-off transition being about one third of that for the fundamental transition. Indeed, using the CP parabolic band model of Adachi, one finds that the oscillator strength is proportional to $\mu^{3/2}$, where μ is the reduced effective mass, whereas selection rules dictate that the split-off oscillator strength is one half the oscillator strength of the light- and heavy-hole bands.^{56,57} Using the combined effective mass of light and heavy holes,⁵⁸ and the effective mass for the split-off band, one finds that S_{rel} equals 0.34 for GaAs. This number is very close to the experimental value of 0.32 indicated in Table III.

Both the S_{rel} and O_{rel} values for the $E_+\Delta_{so}$ transition increase monotonically with x by about a factor of about 3 over the N composition range investigated. This behavior is a strong indication that valence bands are also affected by the presence of nitrogen. Indeed, if the valence bands were unaffected by the presence of N, the $E_+\Delta_{so}$ transition should follow the same trend as the E_- transition, since the same conduction band is involved in both $E_+\Delta_{so}$ and E_- transitions. The different behavior depicted in Fig. 8(b) for the $E_+\Delta_{so}$ transition therefore indicates a stronger perturbation of the valence bands with nitrogen than what has previously

been envisioned. Our data also suggest that the upper lying valence bands and their split-off replica are affected differently.

Since the oscillator strength of the E_- transition increases only weakly, as deduced from a comparison of the absorption coefficient spectra of Fig. 7, we conclude that the oscillator strength of the $E_- + \Delta_{so}$ transition increases over that of the E_- transition.

The most probable origin of the relative increase in the oscillator strength of the $E_- + \Delta_{so}$ transition compared to that of the E_- transition is a decrease in the split-off band curvature. This would imply an increase in the density of states of the split-off band and thus a higher oscillator strength for that transition. Since both the light-hole and split-off band originate from the $m_j = \pm 1/2$ quantum states and couple with the conduction band, a reduction in the split-off band curvature should then also be accompanied by a lowering of the light-hole band curvature. In the four-band $k.p$ method of Kane for semiconductors with a zincblende structure, for example, a change in m_e^* also leads to a change in the light-hole and heavy-hole effective masses.⁵⁹ However, the heavy-hole band being associated with $m_j = \pm 3/2$ quantum states, it does not couple with the first conduction band.⁵⁹

Moreover, the heavy-hole band effective mass is already considerably higher than that of the other two hole bands in the nitrogen free case ($0.53m_0$ for heavy-holes compared to $0.08m_0$ and $0.15m_0$ for light-holes and split-off holes, respectively, m_0 being the free electron mass).⁵⁸ The corresponding heavy-hole density of states is thus dominant. Thus, the effects of the increasing light-hole effective mass on the oscillator strength of the E_- transition could be masked by the

dominant density of states of the heavy-hole band. Since the heavy-hole band is not involved in the transition between the first conduction band and the split-off band, the modification of the latter band may thus be observed.

V. CONCLUSIONS

Using a combination of PR and VASE measurements, we have investigated the band-structure properties of $\text{GaAs}_{1-x}\text{N}_x$ layers ($0 \leq x \leq 0.016$) on $\text{GaAs}(001)$. We observe that the oscillator strength of the E_- optical transition increases weakly with nitrogen incorporation. Furthermore, we determine that the oscillator strength of not only the E_+ transition but also that of the $E_- + \Delta_{so}$ transition become larger compared to the oscillator strength of the fundamental gap E_- as the N content increases. The latter result leads to profound consequences, since the same conduction band is involved in both the E_- transition and its split-off replica. It reveals that the incorporation of nitrogen in $\text{GaAs}_{1-x}\text{N}_x$ (001) alloys also affects the valence bands, most likely by increasing the effective masses of the split-off and light-hole bands.

ACKNOWLEDGMENTS

The authors acknowledge S. Francoeur for fruitful discussions. This work was supported by the Natural Sciences and Engineering Research Council of Canada (NSERC), the Fonds Québécois de la Recherche sur la Nature et les Technologies (FQRNT), and the Canada Research Chair Program. S.T., J.-N.B., and S.L. acknowledge support from the NSERC and the FQRNT.

- ¹J. F. Geisz and D. J. Friedman, *Semicond. Sci. Technol.* **17**, 769 (2002).
- ²A. Mascarenhas and Y. Zhang, *Curr. Opin. Solid State Mater. Sci.* **5**, 253 (2001).
- ³M. Kondow, T. Kitatani, S. Nakatsuka, M. C. Larson, K. Nakahara, Y. Yazawa, M. Okai, and K. Uomi, *IEEE J. Sel. Top. Quantum Electron.* **3**, 719 (1997).
- ⁴M. Kondow, T. Kitatani, S. Nakatsuka, Y. Yazawa, and M. Okai, *Proceedings of the Second Optoelectronics and Communications Conference, Seoul, 1998* (unpublished), p. 168.
- ⁵G. S. Kinsey, D. W. Gotthold, A. L. Holmes Jr., and J. C. Campbell, *Appl. Phys. Lett.* **77**, 1543 (2000).
- ⁶C. W. Tu, *J. Phys.: Condens. Matter* **13**, 7169 (2001).
- ⁷P. J. Klar, H. Gruning, W. Heimbrodt, G. Weiser, J. Koch, K. Volz, W. Stolz, S. W. Koch, S. Tomic, S. A. Choulis, T. J. C. Hosea, E. P. O'Reilly, M. Hofmann, J. Hader, and J. V. Moloney, *Semicond. Sci. Technol.* **17**, 830 (2002).
- ⁸J. Endicott, A. Patane, J. Ibanez, L. Eaves, M. Bissiri, M. Hopkinson, R. Airey, and G. Hill, *Phys. Rev. Lett.* **91**, 126802 (2003).
- ⁹C. Skierbiszewski, S. P. Lepkowski, P. Perlin, T. Suski, W. Jantsch, and J. Geisz, *Physica E (Amsterdam)* **13**, 1078 (2002).
- ¹⁰W. Shan, W. Walukiewicz, J. W. I. Ager, E. E. Haller, J. F. Geisz, D. J. Friedman, J. M. Olson, and S. R. Kurtz, *Phys. Rev. Lett.*

82, 1221 (1999).

- ¹¹A. Mascarenhas, S. Francoeur, and S. Yoon, *Dilute Nitride Semiconductors* (Elsevier, Amsterdam, 2005), Chap. 6, p. 179.
- ¹²S. Francoeur, M. J. Seong, M. C. Hanna, J. F. Geisz, A. Mascarenhas, H. P. Xin, and C. W. Tu, *Phys. Rev. B* **68**, 075207 (2003).
- ¹³W. Shan, W. Walukiewicz, K. M. Yu, J. W. I. Ager, E. E. Haller, J. F. Geisz, D. J. Friedman, J. M. Olson, S. R. Kurtz, H. P. Xin, and C. W. Tu, *Phys. Status Solidi B* **223**, 75 (2001).
- ¹⁴B. Fluegel, A. Mascarenhas, A. J. Ptak, S. Tixier, E. C. Young, and T. Tiedje, *Phys. Rev. B* **76**, 155209 (2007).
- ¹⁵J. Sik, M. Schubert, G. Leibiger, V. Gottschalch, and G. Wagner, *J. Appl. Phys.* **89**, 294 (2001).
- ¹⁶G. Leibiger, V. Gottschalch, V. Riede, M. Schubert, J. N. Hilfiker, and T. E. Tiwald, *Phys. Rev. B* **67**, 195205 (2003).
- ¹⁷J. Sik, M. Schubert, G. Leibiger, V. Gottschalch, G. Kirpal, and J. Humlicek, *Appl. Phys. Lett.* **76**, 2859 (2000).
- ¹⁸J. Wagner, K. Köhler, P. Ganser, and N. Herres, *Appl. Phys. Lett.* **77**, 3592 (2000).
- ¹⁹G. Leibiger, V. Gottschalch, B. Rheinländer, J. Šik, and M. Schubert, *J. Appl. Phys.* **89**, 4927 (2001).
- ²⁰S. Matsumoto, H. Yaguchi, S. Kashiwase, T. Hashimoto, S. Yoshida, D. Aoki, and K. Onabe, *J. Cryst. Growth* **221**, 481 (2000).

- ²¹P.-W. Li, H.-C. Guang, and N.-Y. Li, *Jpn. J. Appl. Phys., Part 2* **39**, L898 (2000).
- ²²G. Leibiger, V. Gottschalch, and M. Schubert, *J. Appl. Phys.* **90**, 5951 (2001).
- ²³C. Skierbiszewski, P. Perlin, P. Wisniewski, T. Suski, J. F. Geisz, K. Hingerl, W. Jantsch, D. E. Mars, and W. Walukiewicz, *Phys. Rev. B* **65**, 035207 (2001).
- ²⁴W. K. Hung, M. Y. Chern, Y. F. Chen, Z. L. Yang, and Y. S. Huang, *Phys. Rev. B* **62**, 13028 (2000).
- ²⁵N. B. Sedrine, J. Rihani, J. L. Stehle, J. C. Harmand, and R. Chtourou, *Mater. Sci. Eng., C* **28**, 640 (2008).
- ²⁶V. Timoshevskii, M. Côté, G. Gilbert, R. Leonelli, S. Turcotte, J.-N. Beaudry, P. Desjardins, S. Larouche, L. Martinu, and R. A. Masut, *Phys. Rev. B* **74**, 165120 (2006).
- ²⁷P. Cova, R. A. Masut, J. F. Currie, A. Bensaada, R. Leonelli, and C. A. Tran, *Can. J. Phys.* **69**, 412 (1991).
- ²⁸J.-N. Beaudry, R. A. Masut, P. Desjardins, P. Wei, M. Chicoine, G. Bentoumi, R. Leonelli, F. Schiettekatte, and S. Guillon, *J. Vac. Sci. Technol. A* **22**, 771 (2004).
- ²⁹J. A. Woollam, B. Johs, C. M. Herzinger, J. Hilfiker, R. Synowicki, and C. L. Bungay, *Optical Metrology* (SPIE Optical Engineering Press, Bellingham, 1999), Volume CR72, p. 1.
- ³⁰B. Johs, J. A. Woollam, C. M. Herzinger, J. Hilfiker, R. Synowicki, and C. L. Bungay, *Optical Metrology* (SPIE Optical Engineering Press, Bellingham, 1999), Volume CR72, p. 29.
- ³¹S. Takagi, *Acta Crystallogr.* **15**, 1311 (1962).
- ³²D. Taupin, *Bull. Soc. Fr. Mineral. Cristallogr.* **88**, 469 (1964).
- ³³J.-N. Beaudry, N. Shtinkov, R. A. Masut, P. Desjardins, and R. J. J. Rioboo, *J. Appl. Phys.* **101**, 113507 (2007).
- ³⁴D. E. Aspnes, *Surf. Sci.* **37**, 418 (1973).
- ³⁵L. Long and J. Schreiber, *Thin Solid Films* **450**, 60 (2004).
- ³⁶D. E. Aspnes and J. E. Rowe, *Solid State Commun.* **8**, 1145 (1970).
- ³⁷J. Misiewicz, P. Sitarek, G. Sek, and R. Kudrawiec, *Mater. Sci.* **21**, 263 (2003).
- ³⁸S. Zollner, *J. Appl. Phys.* **90**, 515 (2001).
- ³⁹P. Lautenschlager, M. Garriga, S. Logothetidis, and M. Cardona, *Phys. Rev. B* **35**, 9174 (1987).
- ⁴⁰See EPAPS Document No. E-PRBMDO-80-039932 for the average pseudodielectric function of the dilute nitrides samples studied. For more information on EPAPS, see <http://www.aip.org/pubservs/epaps.html>.
- ⁴¹B. Johs, C. M. Herzinger, J. H. Dinan, A. Cornfeld, and J. D. Benson, *Thin Solid Films* **313-314**, 137 (1998).
- ⁴²C. C. Kim, J. W. Garland, H. Abad, and P. M. Raccach, *Phys. Rev. B* **45**, 11749 (1992).
- ⁴³S. Zollner, *Appl. Phys. Lett.* **63**, 2523 (1993).
- ⁴⁴E. B. Brown, *Modern Optics* (Reinhold, New York, 1965), Chap. 3, p. 114.
- ⁴⁵G. Leibiger, V. Gottschalch, B. Rheinländer, J. Šik, and M. Schubert, *Appl. Phys. Lett.* **77**, 1650 (2000).
- ⁴⁶The starting values for the best-match data calculation are selected in the following way: energies are taken from the results of PR best-match calculated data for the three CPs, widths and amplitudes of the E_- and $E_- + \Delta_{so}$ CPs are those of GaAs [WVASE32 software, University Nebraska-Lincoln (UNL) database]; the starting parameters of the split-off transition also serve as the starting parameters for the E_+ CP (except the energy). Unless the VASE best-match calculated data can be improved by letting the energy parameter to vary for a given transition, this parameter is fixed to that obtained from the corresponding PR fit, due to the very good agreement between the transition energies found for both experimental techniques. This again allows the reduction in VASE best-match calculation parameters.
- ⁴⁷J. A. Woollam Co. WVASEW32 software.
- ⁴⁸A. Pulzara-Mora, E. Cruz-Hernandez, J. Rojas-Ramirez, R. Contreras-Guerrero, M. Melendez-Lira, C. Falcony-Guajardo, M. A. Aguilar-Frutis, and M. Lopez-Lopez, *J. Cryst. Growth* **301-302**, 565 (2007).
- ⁴⁹A. Pulzara-Mora, M. Melendez-Lira, C. Falcony-Guajardo, M. Lopez-Lopez, M. A. Vidal, S. Jimenez-Sandoval, and M. A. Aguilar-Frutis, *J. Vac. Sci. Technol. B* **24**, 1591 (2006).
- ⁵⁰U. Tisch, E. Finkman, and J. Salzman, *Phys. Rev. B* **65**, 153204 (2002).
- ⁵¹N. Gonzalez Szwacki and P. Boguslawski, *Phys. Rev. B* **64**, 161201(R) (2001).
- ⁵²N. Shtinkov, P. Desjardins, and R. A. Masut, *Phys. Rev. B* **67**, 081202(R) (2003).
- ⁵³M. D. Sturge, *Phys. Rev.* **127**, 768 (1962).
- ⁵⁴S. Turcotte, J.-N. Beaudry, R. A. Masut, P. Desjardins, G. Bentoumi, and R. Leonelli, *J. Appl. Phys.* **104**, 083511 (2008).
- ⁵⁵R. Kudrawiec, G. Sek, K. Ryczko, J. Misiewicz, and J. C. Harmand, *Appl. Phys. Lett.* **84**, 3453 (2004).
- ⁵⁶S. Adachi, *Phys. Rev. B* **35**, 7454 (1987).
- ⁵⁷S. Adachi, *Physical Properties of III-V Semiconductor Compounds InP, InAs, GaAs, GaP, InGaAs, and InGaAsP* (Wiley, New York, 1992), Chap. 8, p. 147.
- ⁵⁸P. Y. Yu and M. Cardona, *Fundamentals of Semiconductors: Physics and Materials Properties* (Springer-Verlag, New York, 2001), Chap. 2, p. 75.
- ⁵⁹G. Bastard, *Wave Mechanics Applied to Semiconductor Heterostructures* (Les Editions de Physique, Les Ulis, 1988), Chap. 2, p. 46.